CATALYSIS

Ternary NiMo-Bi liquid alloy catalyst for efficient hydrogen production from methane pyrolysis

Luning Chen[1]†, Zhigang Song[1,2]†, Shuchen Zhang[1], Chung-Kai Chang[3], Yu-Chun Chuang[3], Xinxing Peng[1], Chaochao Dun[4], Jeffrey J. Urban[4], Jinghua Guo[5], Jeng-Lung Chen[3]*, David Prendergast[4], Miquel Salmeron[1], Gabor A. Somorjai[1,6]*, Ji Su[1,7]*

Methane pyrolysis (MP) is a potential technology for CO_2-free hydrogen production that generates only solid carbon by-products. However, developing a highly efficient catalyst for stable methane pyrolysis at a moderate temperature has been challenging. We present a new and highly efficient catalyst created by modifying a Ni-Bi liquid alloy with the addition of Mo to produce a ternary NiMo-Bi liquid alloy catalyst (LAC). This catalyst exhibited a considerably low activation energy of 81.2 kilojoules per mole, which enabled MP at temperatures between 450 and 800 Celsius and a hydrogen generation efficiency of 4.05 ml per gram of nickel per minute. At 800 Celsius, the catalyst exhibited 100% H_2 selectivity and 120 hours of stability.

H ydrogen (H_2) is emerging as a promising clean energy solution on a global scale (1–3). However, most H_2 production (90 million tons in 2020) comes from fossil fuels, such as natural gas, oil, and coal, which result in substantial CO_2 emissions (about 900 million tons) (4). Water electrolysis is a green H_2 technology that uses renewable energy to produce CO_2-free H_2 (5). However, currently it only contributes 2% of H_2 production given its high cost (5 to 6 USD per kg_{H_2}) and high energy consumption (286 kJ/mol_{H_2}) (6). Methane (CH_4) pyrolysis (MP) is another CO_2-free method for H_2 production that in addition produces valuable carbon materials, such as graphene, carbon nanotubes, and fullerenes (7). Although the MP reaction requires only 37.5 kJ

of energy to produce one mole of H_2, it still requires high reaction temperatures (>1000°C) to activate CH_4, leading to high energy demand, costly equipment, and unavoidable heat losses (8, 9). Moderate reaction temperature would mitigate by-product formation (ethane, ethylene, acetylene, aromatics), minimizing H_2 separation and purification operations. Thus, it is essential to develop optimal catalysts that exhibit high catalytic activity, enabling a moderate operating temperature while also demonstrating excellent resistance to fouling and degradation.

Traditional supported transition metal catalysts (Ni, Co, Fe, Pt, or Pd) can catalyze MP under appropriate low reaction temperatures (500 to 600°C) with low apparent activation energy (Ea) values ranging from 65 to 96 kJ/mol,

but they invariably suffer from deactivation carbon coking and aromatics fouling (10,). Molten liquid catalysts (MLCs) can overcome the deactivation issue by removing carbon products that float on top of the liquid catalysts and offer excellent durability. However, the high E_a of MLCs, ranging from 160 to 310 kJ/mol, demands high temperatures for CH_4 activation (Fig. 1A) (12–14).

Recent findings indicated that the Ni-Bi liquid alloy metal catalyst could catalyze MP. However, the strong interaction between the active metal sites and solvent metal created a cage with positively charged Bi atoms encapsulating negative charged Ni. This atomic arrangement obstructs the CH_4 reaction and results in low activity with a high activation energy E_a of 208 kJ/mol (15). Hence, reducing the cage effect of liquid metal catalysts is crucial to achieving a highly active catalyst for MP. Although liquid-metal catalysts have been used as new-generation catalysts in some specific catalytic processes (16–18), so far

[1]Chemical Sciences Division, Lawrence Berkeley National Laboratory, Berkeley, CA 94720, USA. [2]John A. Paulson School of Engineering and Applied Sciences, Harvard University, Cambridge, MA 02138, USA. [3]National Synchrotron Radiation Research Center, Science-Based Industrial Park Hsinchu 300092, Taiwan. [4]Molecular Foundry, Lawrence Berkeley National Laboratory, Berkeley, CA 94720, USA. [5]Advanced Light Source, Lawrence Berkeley National Laboratory, Berkeley, CA 94720, USA. [6]Department of Chemistry, University of California-Berkeley, Berkeley, CA 94720, USA. [7]Energy Storage and Distributed Resources Division, Lawrence Berkeley National Laboratory, Berkeley, CA 94720, USA.
*Corresponding author. Email: chen.jl@nsrrc.org.tw (J.-L.C.); somorjai@berkeley.edu (G.A.S.); jisu@lbl.gov (J.S.)
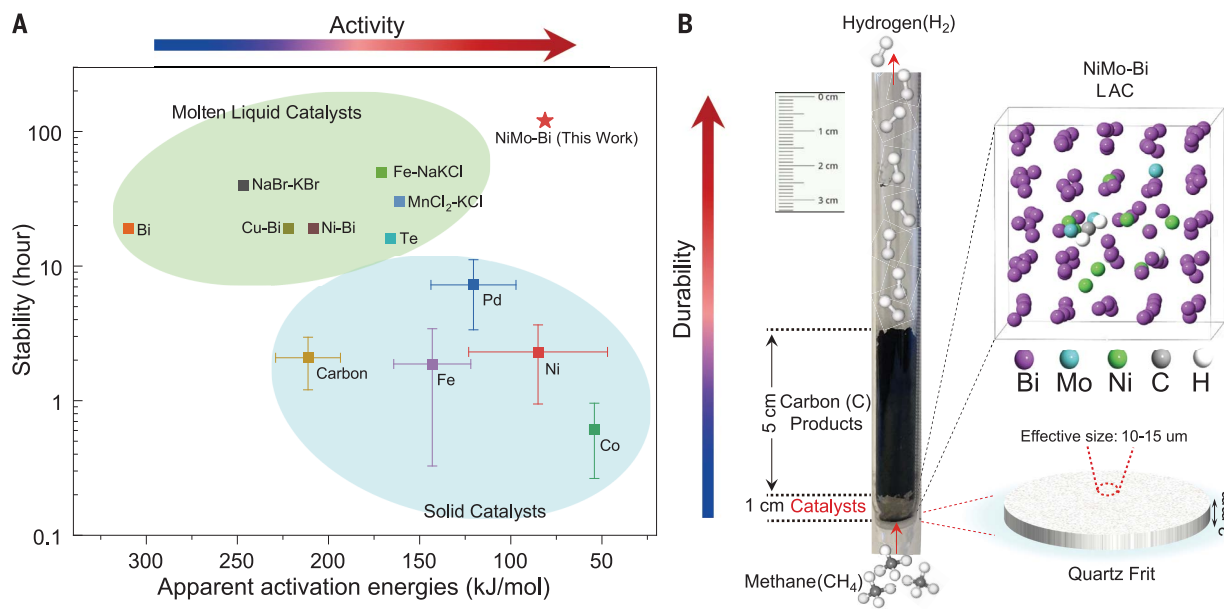†These authors contributed equally to this work.

Fig. 1. Scheme of H_2 production from CH_4 pyrolysis. (**A**) Overview of catalysts for H_2 production from CH_4 pyrolysis, including the stability and activity of different solid and molten liquid catalysts. (**B**) Image of cooling down reactor after a long-time CH_4 pyrolysis reaction (detailed parameters and images in figs. S1 and S2).
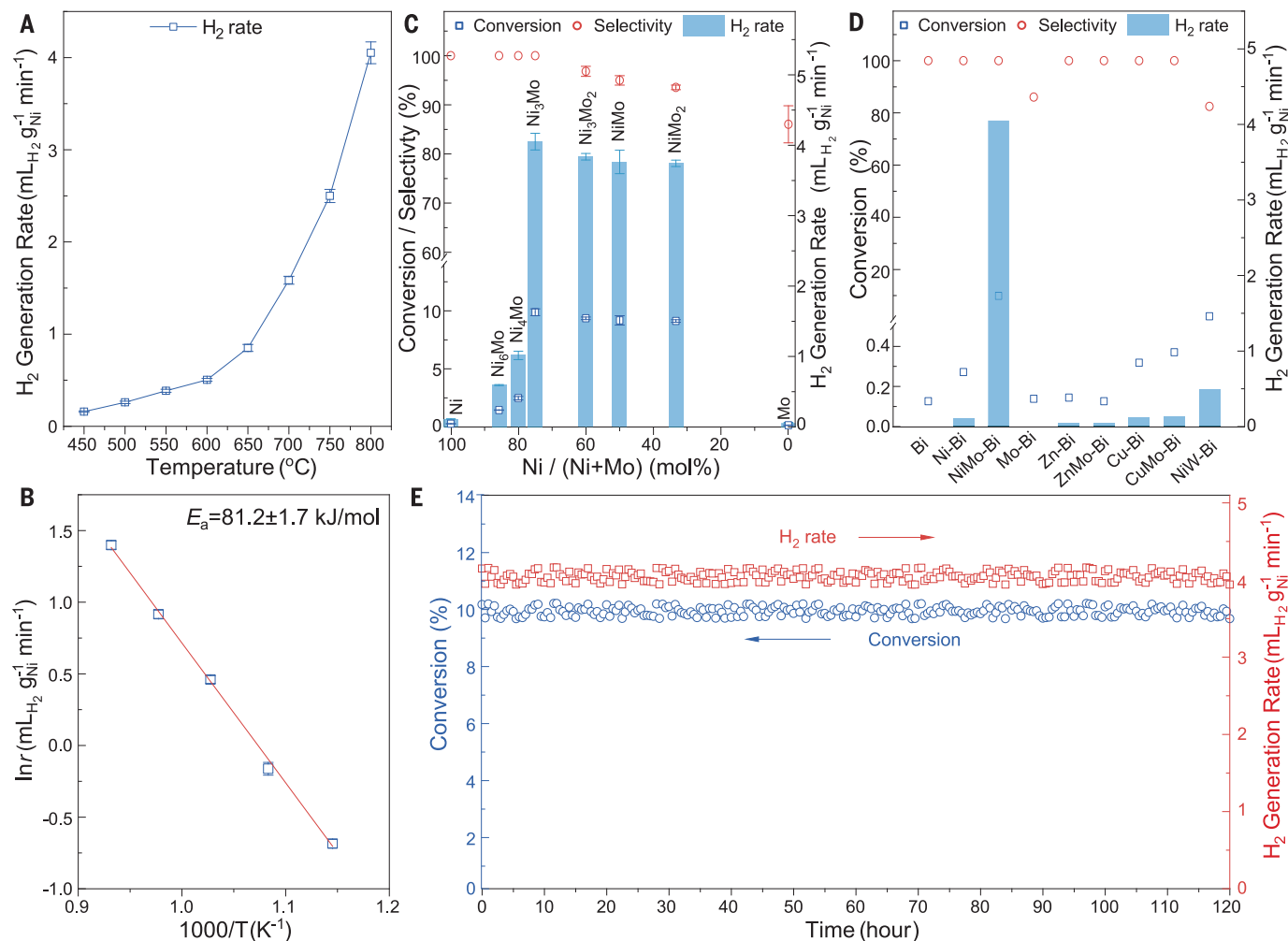
Fig. 2. Catalytic data. (A) H₂ generation rate under different reaction temperatures and **(B)** the apparent activation energy of CH₄ pyrolysis over NiMo-Bi liquid alloy catalyst (with a molar ratio of Ni to Mo of 3:1). Reaction conditions: 4 ml/min CH₄, pressure: 206 kPa (30 psi), catalyst height: <1 cm. **(C)** The conversion and selectivity (left) and H₂ generation rate (right) at 800°C over NiMo-Bi LAC with different composition. All catalysts contain the same Ni amount. **(D)** The conversion and selectivity (left) and H₂ generation rate (right) at 800°C over different liquid metal alloy catalysts. **(E)** The long-time stability measurement of CH₄ dehydrogenation over NiMo-Bi LAC (with a molar ratio of Ni to Mo of 3:1) at 800°C with 4 ml/min CH₄.

studies have not focused on tailoring the interaction between active sites and surrounding solution metal.

NiMo-Bi liquid alloy catalyst for MP

Compared with single-element metal materials, multi-element alloys have attracted attention in recent years because of their mechanical, physical, and chemical properties resulting from the entropy increase (19–21). The properties of alloy catalysts can be modified by additional elements, similar to how soluble metal complex catalysts can be modified by tuning ligands to modify active sites and their interaction with solvents (22–24). We added the third metal to regulate the interaction between the active metal and solution metals. We found that the introduction of Mo successfully decreases the cage effect from Bi atoms surrounding the Ni (15), as a result of the Ni-Mo interaction (Fig. 1B). The NiMo-Bi (Ni 2.3 wt %, Mo 1.3 wt %, and Bi

96.4 wt %) catalysts displayed the maximum MP activity with a high H₂ generation efficiency (4.05 mL$_{H2}$ g$_{Ni}^{-1}$ min^{-1}) at 800°C, which is 37 times faster than Ni-Bi catalysts. The E_a of our NiMo-Bi catalyst was 81.2 kJ/mol, substantially lower than other reported MLCs, approaching the level of supported solid metal catalysts (65 to 96 kJ/mol).

The preparation process of the NiMo-Bi catalyst was simple. For example, the best-performing NiMo-Bi catalyst (with an Ni-to-Mo molar ratio of 3:1) was prepared by directly reducing a mixture of nickel oxide, molybdenum oxide, and bismuth pellets in a quartz reactor with H₂ gas (figs. S1 and S2) (see details in supporting information). After the reduction, the mixture melted into the liquid metal solution under N₂ and was ready to be used for the MP reaction. We used high-resolution powder x-ray diffraction (XRD) to identify the structure of the liquid NiMo-Bi catalyst after cooling down to room

temperature under an inert atmosphere. We identified a major crystal Bi phase with a symmetry group of *R-3m* (ICSD-64703), and a minor Bi₃Ni phase with *Pnma* symmetry (ICSD-391336) according to the fitting results (fig. S3) (25). No appreciable amounts of phases related to the Mo component were detected compared with the Ni-Bi sample. We found that the Ni-Mo interaction could enhance the solubility of Mo in Bi, and more evidence will be provided in the spectroscopy and theoretical study sections. We next studied the phase transitions in a melting process by in situ high-temperature XRD (fig. S4). The crystal phase of Bi disappeared at 260°C near the Bi melting point of 270°C. The Bi₃Ni phase disappeared at 420°C (26), indicating that above this temperature, the NiMo-Bi catalyst remained in the liquid state, with Ni and Mo homogeneously distributed in the liquid solution (fig. S5). In situ high-temperature energy-dispersive spectroscopy mapping showed that
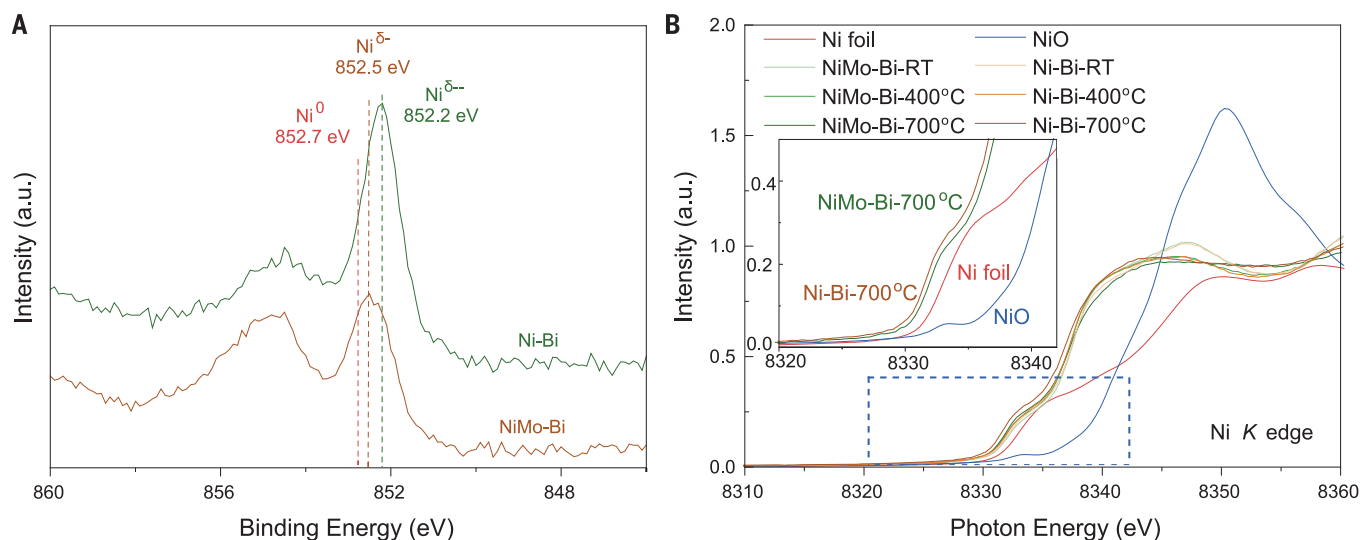
Fig. 3. Statement of Ni species of Ni-Bi and NiMo-Bi liquid alloy catalysts. (**A**) Nickel 2p x-ray photoelectron spectroscopy (XPS) of Ni-Bi and NiMo-Bi catalysts at room temperature. (**B**) Ni K-edge x-ray absorption near edge spectroscopy (XANES) spectra of Ni-Bi and NiMo-Bi catalysts at room temperature (RT) and operating temperature.

Fig. 4. Molecular dynamics simulation. (**A**) Average transferred electrons to a Ni atom. Molecular dynamics is performed using alloys of Ni-Bi and NiMo-Bi at 1500 K. (**B**) H atomic number around a C atom as a function of time. Molecular dynamics is performed using a CH_4 molecule in the alloy of NiMo-Bi and Ni-Bi at 1500 K. (**C**) Snaps of CH_4 in the liquid alloy of Ni-Bi and NiMo-Bi (detailed process in movies S5 and S6).
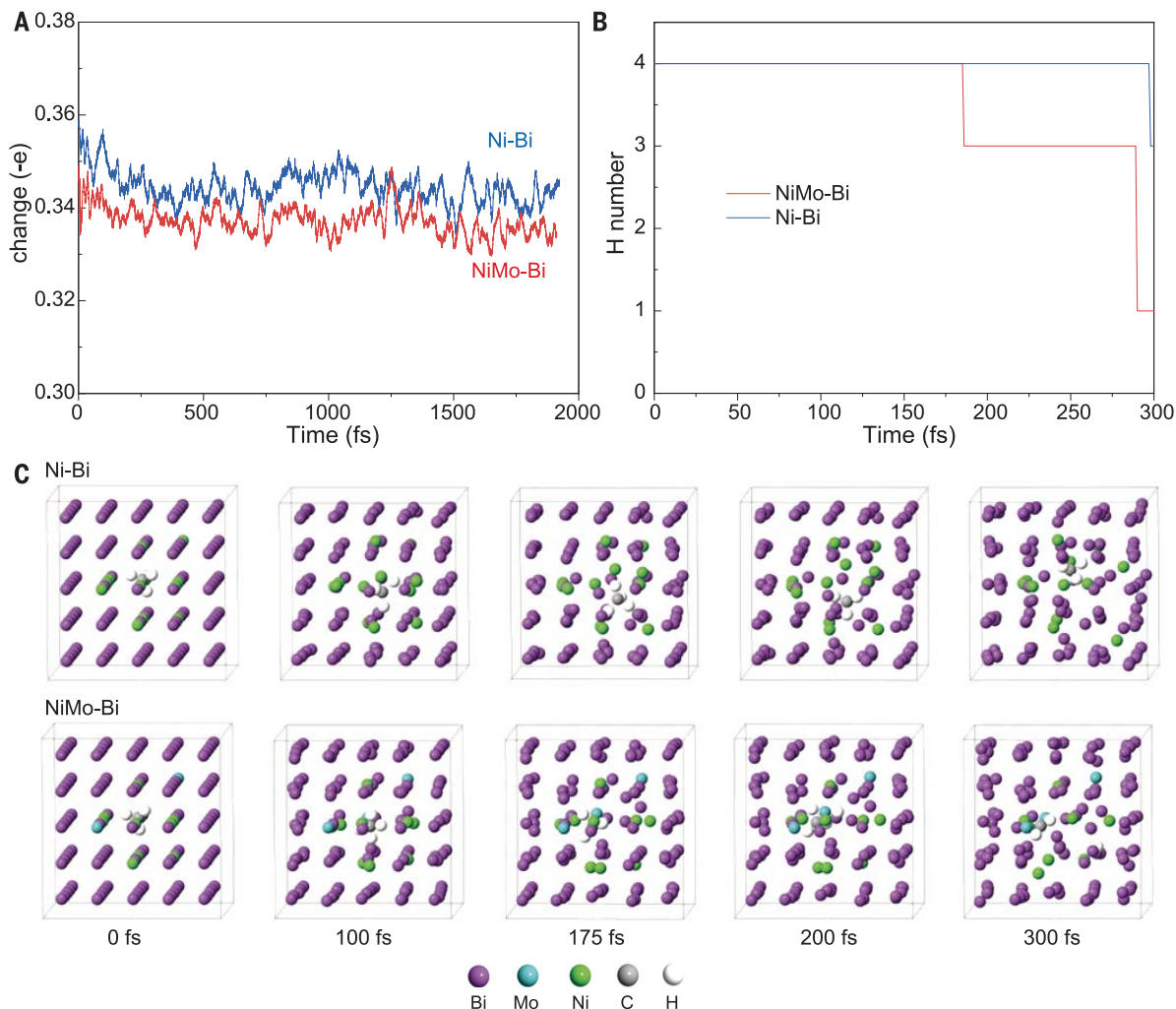
at 500°C., the Ni, Mo, and Bi were uniformly distributed in the liquid alloy (fig. S6).

Catalytic studies

After catalyst preparation, CH_4 was introduced in the reactor and passed through the liquid catalyst to investigate the MP performance at different temperatures with a flow rate of 4 ml/min CH_4 and a 206 kPa (30 psi) pressure. The residence time of CH_4 through the liquid alloy catalyst was around 0.13 min.

No H_2 was detected below 400°C. At 450°C, the catalysts were completely melted (fig. S5), and H_2 was detected with a generation rate of 0.16 mL$_{H2}$ g$_{Ni}^{-1}$ min^{-1}. High temperature favored H_2 production and CH_4 conversion. Increasing the temperature to 800°C, the H_2 generation rate increased to 4.05 mL$_{H2}$ g$_{Ni}^{-1}$ min^{-1} and the CH_4 conversion reached 9.87% (Fig. 2A), which is 37 times higher than the Ni-Bi catalyst (0.11 mL$_{H2}$ g$_{Ni}^{-1}$ min^{-1}). No other by-products were detected under the operation temperatures (fig. S7), indicating complete CH_4 decomposition. Notably, this reaction system avoided the production of aromatics that result in fouling by acetylene by-products, which would cause catalyst deactivation and reaction blocking (27, 28). The E_a of 81.2 kJ/mol was determined from the Arrhenius plots (Fig. 2B). This value is much lower than in all reported MLCs (166 to 310 kJ/mol) and comparable to that of solid metal catalysts (13).

The catalytic MP performance was further investigated under different reaction conditions (fig. S8). Lower flow rates or CH_4 concentration led to an increase in CH_4 conversion. When the CH_4 flow rate decreased to 1 ml/min, the conversion of CH_4 increased to 11.2%. Increasing the CH_4 pressure to 310 kPa (45 psi), the CH_4 conversion increased to 13.1% as a result of CH_4 solubility enhancement. Notably, the residence time of CH_4 could be tuned by the catalyst height. Longer residence times increase the CH_4 conversion. For a 5-cm-tall NiMo-Bi catalyst column, CH_4 conversion raised to 16.3%, which is higher compared with previous Ni-Bi catalysts (13%) even with higher catalyst columns (8 cm) and higher temperature (1000°C) (15). When 10% CH_4 diluted in N_2 was fed into the 5-cm-tall NiMo-Bi catalyst, the CH_4 conversion could reach up to 51.7% under 800°C and 2 bar of total pressure. These results indicated that CH_4 conversion could be further enhanced by reactor engineering optimization. Considering the considerably higher activity of our catalyst and similar catalyst physical properties to the Ni-Bi catalyst (15), it is reasonable to assume that achieving a conversion close to the reaction equilibrium is feasible.

To determine the effect of different elements on catalytic results, we investigated the performance of liquid alloy catalysts with different Ni-Mo-Bi ratios (Fig. 2C and S9). Pure liquid Bi displayed no measurable activity for MP below

800°C. The Ni-Bi catalyst (without Mo) generated H_2 at a rate of 0.02 mL$_{H2}$ g$_{Ni}^{-1}$ min^{-1} starting at 650°C, which increased to 0.11 mL$_{H2}$ g$_{Ni}^{-1}$ min^{-1} at 800°C. Introducing Mo increased the reaction activity and reduced the onset temperature for MP. The H_2 generation rate over the Ni$_6$Mo-Bi catalyst was 0.59 mL$_{H2}$ g$_{Ni}^{-1}$ min^{-1} at 800°C and reached 1.02 mL$_{H2}$ g$_{Ni}^{-1}$ min^{-1} for Ni$_4$Mo-Bi. The best catalytic performance was achieved at a ratio of Ni to Mo of 3:1. As the concentration of Mo was further increased, the H_2 generation rate slightly decreased, whereas the H_2 selectivity also decreased because of the formation of hydrocarbon by-products. These results demonstrate that in the NiMo-Bi liquid alloy system Ni was the active metal, with Bi acting as the solvent. Further, Mo, which has strong interaction with Ni, performed as the regulatory metal and enhanced the reaction activity by modulating the interaction of the solvent Bi metal and the active Ni metal.

We further investigated liquid alloy catalyst systems of different compositions, all in the liquid phase under the reaction temperature (Fig. 2D and fig. S10). No catalytic activity was detected for either Zn-Bi or ZnMo-Bi catalysts. The Cu-Bi catalyst had similar catalytic activity to Ni-Bi (29). However, in contrast to the NiMo-Bi system, the addition of Mo did not appreciably enhance the reaction activity of the CuMo-Bi catalyst. Furthermore, when W was used instead of Mo in the NiMo-Bi system, despite its similar chemical and physical properties, the enhancement observed was much smaller compared with Mo, especially at high temperatures, due to the weaker interaction between Ni and W compared to that between Ni and Mo (30).

In addition to high activity and selectivity, the NiMo-Bi catalyst also exhibited excellent stability in the MP reaction. After 120 hours of measurement at 800°C with a methane flow rate of 4 ml/min, the NiMo-Bi maintained excellent activity and selectivity without any deactivation relative to the initial performance (Fig. 2E), which is better than most MP catalysts including MLCs and traditional solid catalysts (Fig. 1A). The Ni and Mo were still uniformly dispersed in the Bi solution without any aggregation, suggesting that the NiMo-Bi could maintain stability over an even longer period. During the reaction, the carbon product was segregated from the catalysts and accumulated on the catalyst surface (fig. S11). No sticky aromatic fouling species were detected on the wall of the quartz reactor. By further washing the carbon products with acetone, no aromatic products were detected by GC-MS. Notably, although the carbon could also catalyze the MP reaction, under our reaction condition the activity of the NiMo-Bi catalyst was much higher than that of the formed carbon, indicating that all MP activity comes from NiMo-Bi catalysts. To further confirm this, 100-mg carbon products were used as a catalyst, which displayed low activity (0.6% conver-

sion) and fast deactivation rate (36% in 5 min) under a similar reaction condition (fig. S12).

Spectroscopy studies

X-ray photoelectron spectroscopy (XPS) and in situ x-ray absorption near-edge spectroscopy (XANES) were applied to further investigate the chemical state of the species in the liquid alloy catalysts. XPS (Fig. 3A) results show that the binding energy of the Ni 2p level in the Ni-Bi catalyst (852.2 eV) was 0.5 eV lower than that of metallic Ni (852.7 eV) (31), indicating that Ni was negatively charged by electron transfer from surrounding Bi, in agreement with previous work (32). After Mo introduction, the peaks of Ni in NiMo-Bi shifted to a higher binding energy (852.5 eV), suggesting that the Ni in NiMo-Bi catalyst is closer to the metallic state but still negatively charged.

In situ high-temperature XANES (fig. S13) was used to explore the Ni electronic structure at the reaction temperature (Fig. 3B and fig. S14). Consistent with XPS results, the adsorption edge energies of Ni in Ni-Bi and NiMo-Bi LACs were lower than that of the Ni reference foil at room temperature, indicating its negative charge resulting from the interaction with Bi (33). Heating up catalysts under an inert atmosphere, the adsorption edge energies of both Ni-Bi and NiMo-Bi moved to lower values, implying that in the liquid state, Ni is well mixed with Bi, favoring electron transfer from Bi to Ni (15, 34). After Mo introduction, the strong interaction between Ni and Mo modulated the electronic state of Ni and reduced the interaction between Ni and Bi (35). Additionally, the XANES spectra of NiMo-Bi at Mo K-edge showed that at both high temperature and room temperature the valence state of Mo is different from that in the metallic foil and molybdenum oxide, which indicated that there is no Mo metal or molybdenum oxide in the liquid alloy. Further, no Mo-Mo or Ni-Ni bonds were detected in the NiMo-Bi liquid alloy according to room temperature extended x-ray absorption fine structure spectra (fig. S15). The different radial distances and coordination environment of Ni and Mo of NiMo-Bi catalysts, compared with metal foil counterparts, further proved that Ni and Mo were uniformly dispersed without any aggregation (36). Moreover, the difference between the Ni-Bi and NiMo-Bi catalysts indicated the interaction between Ni and Mo, which is also different from the traditional Ni-Bi alloy. These spectroscopy studies successfully verified the existence of interactions between Ni and Mo in the NiMo-Bi melt, which resulted in Ni being less negatively charged and the enhancement of Mo solubility in the Ni-Bi system.

Theoretical studies

A theoretical molecular dynamics simulation based on density functional theory was conducted

to gain deeper insights into the electronic structure and reaction process in the liquid alloy catalysts (the details of the calculation are shown in the supplementary information). First, we simulated the dissolution process of the Mo_2 dimer and Mo cluster (fig. S16 and movies S1 and S2). In the pure molten Bi, the distance of two Mo atoms of Mo_2 dimer did not change as a result of the limited solubility of Mo (37), but in the presence of Ni the Mo-Mo distance would increase. Similar results were found in the Mo cluster in Bi-Ni liquid alloy. These results demonstrate that the solubility of Mo could be enhanced as a result of Ni-Mo interaction leading to Mo uniformly dispersing in the liquid alloy instead of aggregating. Then we monitored the average Ni electron charge in Ni-Bi and NiMo-Bi catalysts (Fig. 4A). In accordance with XPS and XANES results, the Ni dissolved in Bi with or without Mo are both negatively charged because of the difference of electron affinity between Ni and Bi. After Mo introduction the charge of the Ni atoms decreased, which could potentially increase the Ni mobility as well as decrease the interaction between Ni and surrounding Bi atoms (38).

To further understand this phenomenon, we embedded a Ni atom in the Bi solution and carried out a molecular dynamics simulation at 1500 K. The Ni atom was surrounded by Bi atoms (fig. S17 and movie S3). However, after Mo introduction, the Ni atom broke through the surrounding Bi atoms, making it more accessible to CH_4 molecules as catalytic active sites (fig. S18 and movie S4). Subsequently, we introduced CH_4 in the NiMo-Bi and Ni-Bi systems to follow the dissociation process at 1500 K (Fig. 4C and movies S5 and S6). The number of H of CH_4 was calculated and the results are listed in Fig. 4B. The strong interaction between Ni and Bi made it more difficult for the CH_4 molecules to reach the caged Ni active sites, resulting in a reaction time to dissociate of about 300 femtosecond (fs) for the Ni-Bi system. However, the introduction of Mo weakened this cage effect and increased the possibility of interaction between Ni and CH_4, which caused CH_4 to start to dissociate at about 180 fs for the NiMo-Bi system. If we introduced W to replace Mo, the CH_4 started to dissociate at 252 fs for NiW-Bi, due to the weak interaction between Ni and W at a high temperature (fig. S19 and movie S7). All

these results are in agreement with our experimental observation.

Discussion

The MP process is widely recognized as a promising approach for clean H_2 production. Nevertheless, it is suffering from a lack of a catalyst capable of efficiently, selectively, and stably catalyzing the MP process under mild reaction temperatures. We developed a NiMo-Bi liquid alloy catalyst that could simultaneously perform high efficiency, selectivity, and durability for methane pyrolysis at mild temperatures.

It is worth noting that the NiMo-Bi liquid alloy catalyst also exhibited high activity for the pyrolysis of other natural gas components, such as ethane and propane (fig. S20). This indicates that this liquid metal alloy catalyst could be further applied in H_2 production from other sources, such as biomass and plastic (39, 40). Further, more-efficient soluble multi-elementary liquid alloy catalysts with different compositions are also under development, which may break through the recent reaction limitations and change the future of catalysis.

REFERENCES AND NOTES

1. L. P. Bicelli, *Int. J. Hydrogen Energy* **11**, 555–562 (1986).
2. "U.S. National Clean Hydrogen Strategy and Roadmap" (United States Department of Energy Press, 2023); https://www.hydrogen.energy.gov/pdfs/us-national-clean-hydrogen-strategy-roadmap.pdf.
3. J. O. Abe, A. P. I. Popoola, E. Ajenifuja, O. M. Popoola, *Int. J. Hydrogen Energy* **44**, 15072–15086 (2019).
4. "HYDROGEN STRATEGY Enabling A Low-Carbon Economy" (Office of Fossil Energy, United States Department of Energy Press, 2020) https://www.energy.gov/sites/prod/files/2020/07/f76/USDOE_FE_Hydrogen_Strategy_July2020.pdf.
5. A. J. Shih *et al.*, *Nat. Rev. Methods Primers* **2**, 84 (2022).
6. O. Schmidt *et al.*, *Int. J. Hydrogen Energy* **42**, 30470–30492 (2017).
7. N. Muradov, *Int. J. Hydrogen Energy* **26**, 1165–1175 (2001).
8. C. Guéret, M. Daroux, F. Billaud, *Chem. Eng. Sci.* **52**, 815–827 (1997).
9. H. F. Abbas, W. W. Daud, *Int. J. Hydrogen Energy* **35**, 1160–1190 (2010).
10. N. S. N. Hasnan *et al.*, *Mater. Renew. Sustain. Energy* **9**, 8 (2020).
11. J. X. Qian *et al.*, *Int. J. Hydrogen Energy* **45**, 15721–15743 (2020).
12. B. Parkinson, J. W. Matthews, T. B. McConnaughy, D. C. Upham, E. W. McFarland, *Chem. Eng. Technol.* **40**, 1022–1030 (2017).
13. M. Msheik, S. Rodat, S. Abanades, *Energies* **14**, 3107 (2021).
14. K. Wang, W. S. Li, X. P. Zhou, *J. Mol. Catal. Chem.* **283**, 153–157 (2008).
15. D. C. Upham *et al.*, *Science* **358**, 917–921 (2017).
16. M. A. Rahim *et al.*, *Nat. Chem.* **14**, 935–941 (2022).
17. N. Taccardi *et al.*, *Nat. Chem.* **9**, 862–867 (2017).
18. K. Kalantar-Zadeh, M. A. Rahim, J. Tang, *Acc. Mater. Res.* **2**, 577–580 (2021).
19. P. C. Chen *et al.*, *Science* **352**, 1565–1569 (2016).
20. E. P. George, D. Raabe, R. O. Ritchie, *Nat. Rev. Mater.* **4**, 515–534 (2019).
21. K. Kusada, M. Mukoyoshi, D. Wu, H. Kitagawa, *Angew. Chem. Int. Ed.* **61**, e202209616 (2022).
22. X. Chen *et al.*, *Nature* **592**, 712–716 (2021).
23. Q. Pan *et al.*, *Science* **374**, 984–989 (2021).
24. W. A. Herrmann, C. W. Kohlpaintner, *Angew. Chem. Int. Ed.* **32**, 1524–1544 (1993).
25. J. Kumar *et al.*, *Supercond. Sci. Technol.* **24**, 085002 (2011).
26. R. Sheikhi, J. Cho, *J. Mater. Sci. Mater. Electron.* **29**, 19034–19042 (2018).
27. A. Jess, *Fuel* **75**, 1441–1448 (1996).
28. X. Guo *et al.*, *Science* **344**, 616–619 (2014).
29. C. Palmer *et al.*, *ACS Catal.* **9**, 8337–8345 (2019).
30. H. Okamoto, P. R. Subramanian, L. Kacprzak, Binary Alloy Phase Diagrams, Second Edition (ASM International, Materials Park, OH, 1990).
31. P. L. Tam, L. Nyborg, *Surf. Coat. Tech.* **203**, 2886–2890 (2009).
32. H. B. Michaelson, *J. Appl. Phys.* **48**, 4729–4733 (1977).
33. B. Das *et al.*, *Phys. Chem. Chem. Phys.* **24**, 4415–4424 (2022).
34. H. Liu *et al.*, *Nat. Catal.* **4**, 202–211 (2021).
35. S. Guo, C. T. Liu, *Prog. Nat. Sci.* **21**, 433–446 (2011).
36. Y. H. Liu *et al.*, *Sci. Adv.* **9**, eadf9931 (2023).
37. A. V. Abramov *et al.*, *Metals (Basel)* **13**, 366–375 (2023).
38. R. Chen *et al.*, *Acta Mater.* **144**, 129–137 (2018).
39. H. Balat, E. Kırtay, *Int. J. Hydrogen Energy* **35**, 7416–7426 (2010).
40. X. Jie *et al.*, *Nat. Catal.* **3**, 902–912 (2020).

SUPPLEMENTARY MATERIALS

science.org/doi/10.1126/science.adh8872
Materials and Methods
Figs. S1 to S21
References (41–44)
Movies S1 to S7

Ternary NiMo-Bi liquid alloy catalyst for efficient hydrogen production from methane pyrolysis

Luning Chen, Zhigang Song, Shuchen Zhang, Chung-Kai Chang, Yu-Chun Chuang, Xinxing Peng, Chaochao Dun, Jeffrey J. Urban, Jinghua Guo, Jeng-Lung Chen, David Prendergast, Miquel Salmeron, Gabor A. Somorjai, and Ji Su

Editor's summary

Very high temperatures are needed to convert methane to hydrogen and solid carbon. A known liquid metal nickel–bismuth catalyst for this pyrolysis reaction resists deactivation but requires reaction temperatures above 1000°C. Chen *et al.* added molybdenum to improve nickel reactivity, which could enable lower operating temperatures. Molybdenum appears to decrease the negative charge on nickel atoms in the molten state and to increase atom mobility and interaction with methane, which enables efficient long-term pyrolysis at 800°C. —Phil Szuromi

View the article online
https://www.science.org/doi/10.1126/science.adh8872
Permissions
https://www.science.org/help/reprints-and-permissions

Use of this article is subject to the Terms of service